

PAPER • OPEN ACCESS

## Description of low-lying collective states in osmium isotopes in the boson expansion theory

To cite this article: Hideo Sakamoto 2020 *J. Phys.: Conf. Ser.* **1555** 012023

View the [article online](#) for updates and enhancements.

You may also like

- [Bohr Hamiltonian with a finite well for triaxial nuclei](#)  
I Inci, I Boztosun and Y E Gonen
- [K-isomers in very neutron-rich nuclei around mass 180](#)  
C Schlegel, P H Regan, M Pfützner et al.
- [Signature of the  \$N = 126\$  shell closure in dwell times of alpha-particle tunneling](#)  
N G Kelkar and M Nowakowski



**ECS**  
The  
Electrochemical  
Society  
Advancing solid state &  
electrochemical science & technology

**DISCOVER**  
how sustainability  
intersects with  
electrochemistry & solid  
state science research

# Description of low-lying collective states in osmium isotopes in the boson expansion theory

**Hideo Sakamoto**

Faculty of Engineering, Gifu University, Gifu 501-1193, Japan

E-mail: sakamoto@gifu-u.ac.jp

**Abstract.** The low-lying collective states in osmium isotopes are investigated microscopically by means of the boson expansion theory with the self-consistent effective interactions. The potential energy surfaces and the structures of boson wave functions are illustrated. Theoretical level structures and electromagnetic properties are compared with the available experimental data. The prolate-oblate shape transition predicted at around  $N = 116$  is also discussed in terms of the evolution of the theoretical potential as the neutron number changes.

## 1. Introduction

Neutron-rich nuclei with  $A \sim 190$  provide a characteristic testing ground for microscopic theories of nuclear structures. There are quite a few indications that a prolate-oblate shape transition takes place at around  $N = 116$  in this region [1, 2, 3].

The boson expansion theory (BET) is a promising method for microscopic description of anharmonicities in nuclear quadrupole collective motions, in terms of the fermion degrees of freedom, if the coupling to non-collective states is faithfully included in the calculation [4, 5]. It allows us to take into account higher-order terms neglected in the RPA, and the adiabatic condition for particle motions can be avoided.

In this paper, the low-lying collective states in osmium isotopes are investigated microscopically by means of the BET with the self-consistent effective interactions [6, 7]. The Kishimoto-Tamura method of normal-ordered linked-cluster expansion of the modified Marumori boson mapping [4] is applied to construct the microscopic boson image of the fermion Hamiltonian and that of the E2 operator. The potential energy surfaces and the structures of boson wave functions [8, 9] for some relevant low-lying collective states are illustrated. Theoretical level structures and electromagnetic properties are compared with the available experimental data.

## 2. Theoretical framework

The theoretical framework is discussed in detail in Refs. [10, 11]; here it is described only briefly.

### 2.1. Fermion description

The model Hamiltonian with which we start is given in fermion operators as

$$H = h_{s.p.} + (H_{0-pair} - \lambda \hat{N}) + H_{2-pair} + V^{(2)} + V^{(3)} + V^{(4)}, \quad (1)$$



with

$$H_{0-pair} = -\frac{G_0}{4}\hat{P}_0^\dagger\hat{P}_0, \quad H_{2-pair} = -\frac{G_2}{2}(\hat{P}_2^\dagger \cdot \hat{P}_2), \quad (2)$$

$$V^{(2)} = -\frac{\chi^{(2)}}{2}(\hat{Q}_2 \cdot \hat{Q}_2), \quad (3)$$

$$V^{(3)} = -\frac{\chi^{(3)}}{3!}[\sqrt{56\pi/5}(\hat{Q}_2\hat{Q}_2\hat{Q}_2) - 3\hat{R}_0(\hat{Q}_2 \cdot \hat{Q}_2)], \quad (4)$$

$$V^{(4)} = -\frac{\chi^{(4)}}{4!}[\frac{48\pi}{5}(\hat{Q}_2 \cdot \hat{Q}_2)^2 - 8\sqrt{56\pi/5}\hat{R}_0(\hat{Q}_2\hat{Q}_2\hat{Q}_2) + 12\hat{R}_0^2(\hat{Q}_2 \cdot \hat{Q}_2)]. \quad (5)$$

Here  $h_{sp}$  is the spherical limit of the Nilsson Hamiltonian [12], and our fermion model space is spanned by  $3s_{1/2}$ ,  $2d_{3/2}$ ,  $2d_{5/2}$ ,  $1g_{7/2}$ ,  $2f_{7/2}$ ,  $1h_{9/2}$ ,  $1h_{11/2}$  and  $1i_{13/2}$  orbits for protons and  $3p_{1/2}$ ,  $3p_{3/2}$ ,  $2f_{5/2}$ ,  $2f_{7/2}$ ,  $1h_{9/2}$ ,  $2g_{9/2}$ ,  $1i_{11/2}$ ,  $1i_{13/2}$  and  $1j_{15/2}$  orbits for neutrons. The residual interactions comprised in the fermion Hamiltonian are the monopole- and quadrupole-pairing interactions,  $H_{0-pair}$  and  $H_{2-pair}$ , the quadrupole-quadrupole (QQ) interaction,  $V^{(2)}$ , and the effective three- and four-body interactions,  $V^{(3)}$  and  $V^{(4)}$ . The effective many-body interactions have been introduced as the higher-order terms of the QQ interaction to recover the saturation and the self-consistency between the density and the potential in higher-order accuracy (*nuclear self-consistency*) [13, 14, 15, 16, 17, 18, 6].

Strengths of the monopole-pairing interactions,  $G_0(p)$  for protons and  $G_0(n)$  for neutrons, are determined to fit the experimental gap energies through the BCS gap equation. The strengths of the quadrupole-pairing interactions are parameterized as  $g'_2(p) = G_2(p)/G_2^{self}(p)$ ,  $g'_2(n) = G_2(n)/G_2^{self}(n)$ , where  $G_2^{self}(p)$  for protons and  $G_2^{self}(n)$  for neutrons are the self-consistent strengths of the quadrupole-pairing interaction to recover the *local Galilean invariance* in the RPA order, respectively [19]. The strengths of the QQ-interaction and its higher-order terms,  $\chi^{(2)}$ ,  $\chi^{(3)}$  and  $\chi^{(4)}$ , are parametrized as  $f_2 = \chi^{(2)}/\chi_2^{self}$ ,  $f_3 = \chi^{(3)}/\chi_3^{self}$ ,  $f_4 = \chi^{(4)}/\chi_4^{self}$ , where  $\chi_2^{self}$ ,  $\chi_3^{self}$  and  $\chi_4^{self}$  are the self-consistent values of  $\chi^{(2)}$ ,  $\chi^{(3)}$  and  $\chi^{(4)}$ , respectively, which are derived in Ref. [6]. In the present analyses, to reduce the number of free parameters, these parameters are set to  $f_2 = f_3 = f_4 = f$  and  $g'_2(p) = g'_2(n) = g'$ , and in calculating the energy spectra the two dimensionless parameters,  $f$  and  $g'$ , are varied slightly around the vicinity of the predicted value, i.e., unity.

## 2.2. Boson description

In the modified Marumori boson mapping [4, 20], orthonormal  $n$  boson states, which span the ideal boson space, are introduced as

$$|n : a\rangle \equiv N(n : a)^{-1}A_{a_1}^\dagger A_{a_2}^\dagger \cdots A_{a_n}^\dagger |0\rangle, \quad (6)$$

where  $A^\dagger$ 's are the ideal boson operators and  $N(n : a)$  is the boson normalization factor with the abbreviated notation  $(n : a) \equiv (a_1, a_2, \cdots, a_n)$  with  $a_1 \leq a_2 \leq \cdots \leq a_n$ . Corresponding  $n$  TD fermion-pair states

$$|n : a \gg \equiv N(n : a)^{-1}B_{a_1}^\dagger B_{a_2}^\dagger \cdots B_{a_n}^\dagger |0 \gg \quad (7)$$

are not generally orthonormal and linearly independent. Here  $B^\dagger$ 's are the TD fermion-pair operators. The fermion norm matrix is denoted as  $\langle\langle n : a | m : b \rangle\rangle \equiv \delta_{nm}(Z_n^2)_{a;b}$ .

In order to construct orthonormalized fermion sates, we have to assume that the inverse of  $Z_n$ , i.e.,  $Z_n^{-1}$ , exists. One of the possible ways would be to divide the fermion space  $\{|n : a \gg\}$

into two parts,  $T_F$  and  $(1 - T_F)$ , i.e., the  $T_F$  space including the components that are retained, and  $(1 - T_F)$  excluding those. Then the ortho-normalized fermion states can be obtained as

$$|n : t \rangle \equiv \sum_{t'} (Z_n^{-1})_{t;t'} |n : t' \rangle; \quad (8)$$

here and in the following  $t, t'$ , etc., indicate the components that belong to the  $T_F$  space while  $\bar{t}, \bar{t}'$ , etc., indicate those that belong to the  $(1 - T_F)$  space. To derive a physically meaningful boson mapping, the ideal boson space  $\{|n : a\rangle\}$  is also divided into two parts,  $T$  and  $(1 - T)$ , i.e., the truncated space  $T$  for boson states is introduced as a replica of the  $T_F$  space for the fermion states.

The one-to-one correspondence between the fermion state  $|n : t \rangle$  and the boson state  $|n : t \rangle$  in the truncated space is obtained by using a mapping operator

$$U = \sum_{(n:t)} |n : t \rangle \langle n : t| \quad (9)$$

as

$$|n : t \rangle = U |n : t \rangle, \quad |n : t \rangle = U^\dagger |n : t \rangle. \quad (10)$$

At the same time, a boson image  $(O_F)_B$  of a fermion operator  $O_F$  is defined by

$$(O_F)_B \equiv U O_F U^\dagger \quad (11)$$

so as to satisfy

$$\langle m : t | O_F |n : t' \rangle = \langle m : t | (O_F)_B |n : t' \rangle \quad (12)$$

in the truncated subspace. The operator  $U$  transcribes the dynamics of a fermion system into that of a boson system.

The normal-ordered linked-cluster expansion of  $(O_F)_B$  is obtained by expressing  $|0\rangle\langle 0|$  and  $(Z_n)_{t;t'}$  in an expansion form. For example, the boson image of the basic TD fermion-pair operator can be expanded as

$$(B_{t_1}^\dagger)_B = A_{t_1}^\dagger - \frac{1}{4} \sum_{t_2 t_3 t_4} Y(t_1 t_2 t_3 t_4) A_{t_2}^\dagger A_{t_3}^\dagger A_{t_4} + O(\epsilon^2), \quad (13)$$

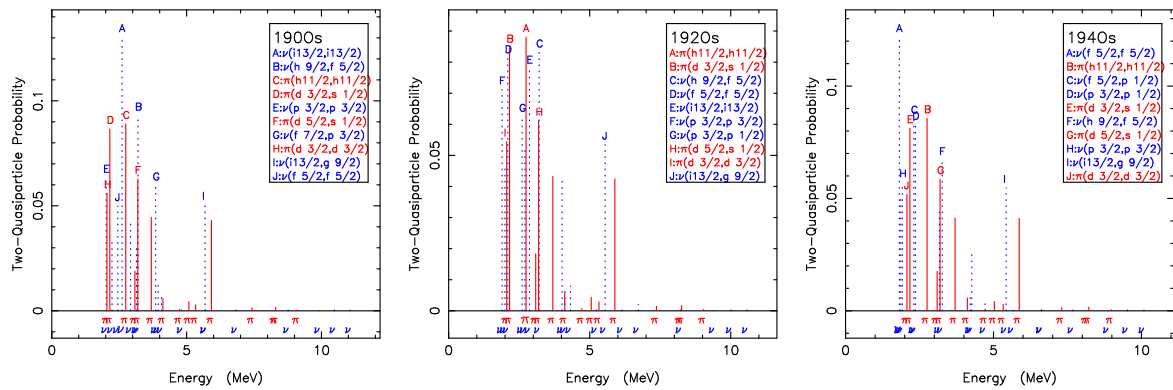
where  $Y(abcd) = 2(Y_2)_{ad;bc}$  with the matrix  $Y_n$  defined by  $Z_n = [1_n - Y_n]^{1/2}$ . The  $\epsilon$  denotes the expansion parameter such as  $|Y_2|$ , and is usually very small if we truncate the system to the collective TD component [4, 20].

In the present numerical calculations, all the TD elements with spin  $I \leq 4$  are regarded as the chosen TD modes, and among them the lowest quadrupole mode is identified as the collective TD mode. Then, by use of the BET, the original fermion Hamiltonian is mapped to the corresponding boson Hamiltonian and is expanded up to fourth-order with respect to the collective boson. Effects of the non-collective branches are included by use of the Feshbach formalism [21] with the closure approximation for the intermediate states in the coupling Hamiltonian [22]. For the collective branch, to include the RPA-type correlations at the early stage of the calculation [22], a transformation from the  $A$  bosons to the so-called  $\alpha$  bosons is introduced as  $A^\dagger = \psi \alpha^\dagger + \phi \tilde{\alpha}$ ,  $\tilde{A} = \phi \alpha^\dagger + \psi \tilde{\alpha}$  with  $\psi^2 - \phi^2 = 1$ . Since the present formalism is based on the quasi-particle representation, the approximate number projection method [20] is carried out to remove the spurious proton- and neutron-pairing rotational modes.

The resultant collective Hamiltonian is diagonalized in the collective subspace of the boson Hilbert space to obtain energy spectra as well as boson wave functions for low-lying collective states. The basis vectors of the collective subspace are expressed as  $|Nv\eta IM\rangle$ , where  $N$  is the boson number,  $v$  is the seniority number,  $I$  is the spin with its projection  $M$ , and  $\eta$  is an additional quantum number necessary for a complete labeling of the basis vectors.

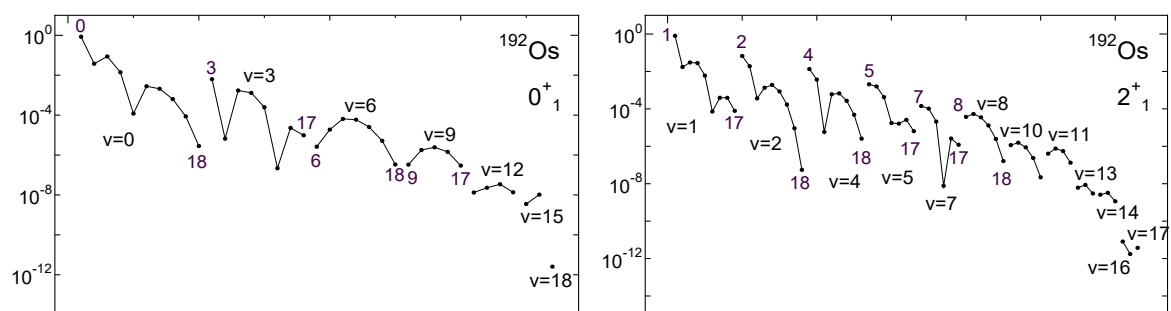
### 3. Results and discussion

Figure 1 shows two-quasiparticle probabilities in the adiabatic collective TD mode [20] calculated for  $^{190,192,194}\text{Os}$ . Since the collective TD mode is the primal building block of the collective boson mode in the present formalism, the evolution of the basic TD mode as the neutron number changes is closely related to the change in the structure of the collective boson, which is essential for the boson description of nuclear structures.



**Figure 1.** (Color online) Two-quasiparticle probabilities in the adiabatic collective Tamm-Dancoff mode for  $^{190,192,194}\text{Os}$  are plotted against the two-quasiparticle energies. The scripts  $\pi$  and  $\nu$  are attached to distinguish the proton components (solid red lines) and the neutron components (dotted blue lines).

In the present numerical calculations, states with  $N \leq 18$  are taken, which amount to a diagonalization space of slightly less than 100-dimensional matrices for each spin  $I$ . Figure 2 presents the structures of the BET wave functions for  $0_1^+$  and  $2_1^+$  states in  $^{192}\text{Os}$ . In this figure one can see to what degree the BET wave functions converge in terms of  $v$  and  $N$  in the numerical calculations. In the boson wave functions of  $^{192}\text{Os}$ , the leading order component of the ground state is  $|N, v\rangle = |0, 0\rangle$  followed by  $|4, 0\rangle, |2, 0\rangle$  and so forth, while that of the  $2_1^+$  state is  $|N, v\rangle = |1, 1\rangle$  followed by  $|2, 2\rangle, |5, 1\rangle$  and so forth.



**Figure 2.** Probability distributions of the boson numbers  $N$  and the seniorities  $v$  in the theoretical wave functions for  $0_1^+$  and  $2_1^+$  states in  $^{192}\text{Os}$ . Components of the same seniority are separately accumulated and connected in the ascending order of  $N$ . The numbers attached at some beginning or ending points represent the boson numbers.

Figure 3(a) illustrates the theoretical potential-energy surface as a function of quadrupole deformation  $\beta$  for  $^{192}\text{Os}$ . This potential surface has two axial minima, one on the prolate side and the other on the oblate side with almost the same depth. This feature of the potential implies

strong softness or instability for the  $\gamma$  deformation. The corresponding theoretical energy levels are presented in Fig.3(b) and compared with experimental levels of Fig.3(c). The energies of the ground-state band and those of the quasi- $\gamma$  band are qualitatively reproduced, though the staggering of quasi- $\gamma$  band is too prominent in the theoretical spectrum.

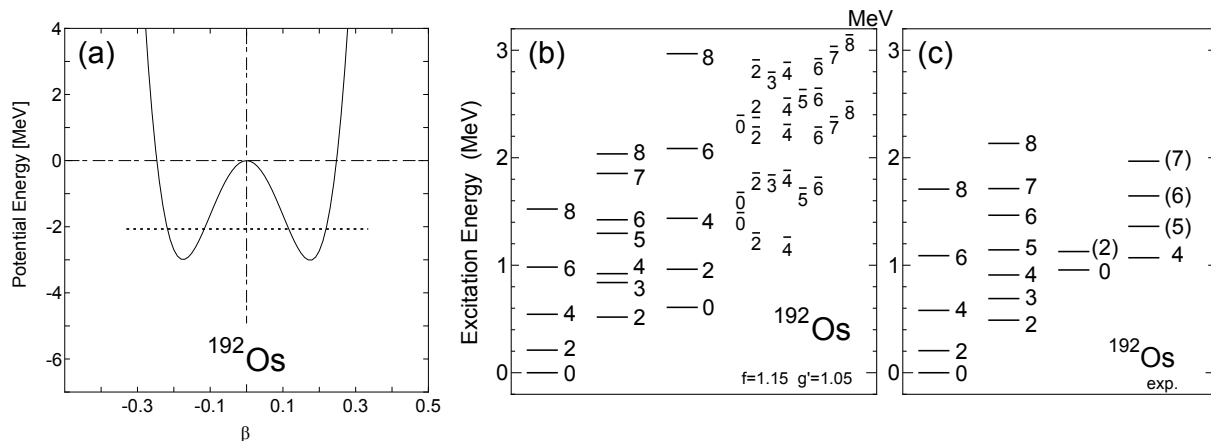


**Figure 3.** (a) Theoretical potential energy surface for  $^{192}\text{Os}$ . The horizontal dotted line indicates the ground-state energy. (b) Theoretical energy levels for  $^{192}\text{Os}$ . The states in the ground-band, the quasi  $\gamma$ -band or the  $0_2^+$  band are separately accumulated, while other states (short bars) are assembled in their spin groups in columnar forms. (c) The experimental spectrum for  $^{192}\text{Os}$  [23].

In Tables 1 and 2, the theoretical  $B(E2)$  values and static quadrupole moments of some low-lying states in  $^{192}\text{Os}$  for the case of  $e_{pol}(E2) = 0.5e$  are listed with experimental data, respectively. These theoretical values reproduce the experimental values almost reasonably except that the difference in the sign of  $Q(2_2^+)$  is a remaining issue.

**Table 1.** Electromagnetic properties of  $^{192}\text{Os}$ . The values given are  $B(E2)$  in  $(e \cdot b)^2$ . An asterisk is attached to a  $B(E2)$  value of the present work (BET) if the sign of the corresponding matrix element is negative.

transition	$I_i$	$I_f$	BET	Exp. [23]
$g \rightarrow g$	2	0	0.415*	$0.409^{+0.004}_{-0.004}$
	4	2	0.610	$0.497^{+0.013}_{-0.013}$
	6	4	0.711	$0.658^{+0.035}_{-0.021}$
	8	6	0.779	$0.757^{+0.038}_{-0.038}$
$\gamma \rightarrow \gamma$	3	2	0.448*	
	4	2	0.420	$0.298^{+0.009}_{-0.012}$
	4	3	0.120*	
$\gamma \rightarrow g$	2	0	0.068	$0.037^{+0.001}_{-0.001}$
	2	2	0.482*	$0.303^{+0.017}_{-0.008}$
	2	4	0.0001	$0.024^{+0.028}_{-0.005}$

**Table 2.** Quadrupole moments for  $^{192}\text{Os}$

Q (eb)	1981Ho [24]	1983Ch [25]	1988Li [26]	BET
$2_1^+$	-0.96(3)	-0.80(18)	-0.86(20)	-0.7678
$2_2^+$	-0.8(3)			0.7963
$4_1^+$				-1.019

For  $^{190}\text{Os}$ , the potential surface, theoretical energy levels and the experimental spectrum are shown in Figs.4(a), 4(b) and 4(c), respectively, while for  $^{194}\text{Os}$ , those are presented in Figs.5(a), 5(b) and 5(c), respectively. Compared with  $^{192}\text{Os}$ , the potential of  $^{190}\text{Os}$  is slightly prolate favored, while that of  $^{194}\text{Os}$  tends to be oblate favored. From Figs.3(a), 4(a) and 5(a), it is inferred that the prolate-oblate shape transition occurs at around  $N = 116$  for osmium isotopes, which is compatible with the prediction of Refs. [1, 2].

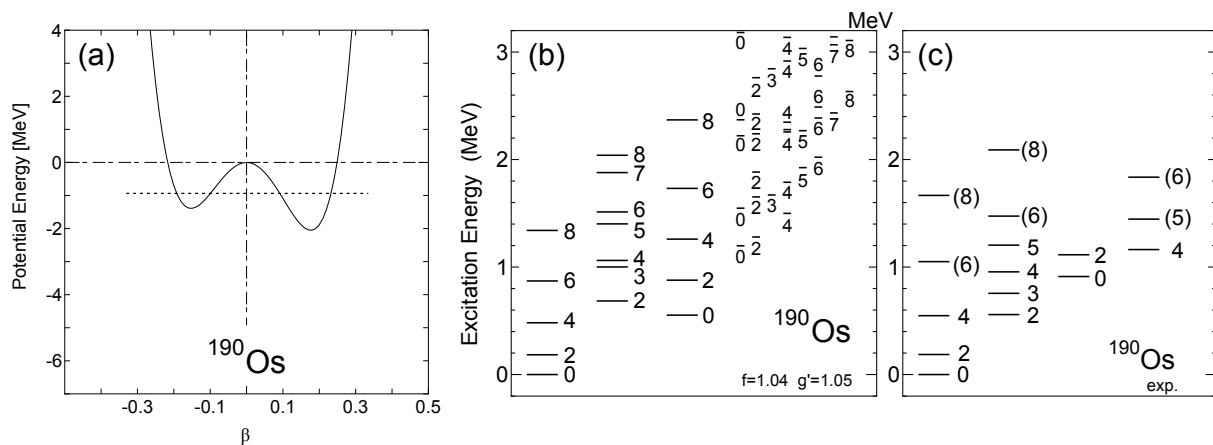


**Figure 4.** Same as Fig. 3 but for  $^{190}\text{Os}$ . Experimental data are taken from Ref.[27].

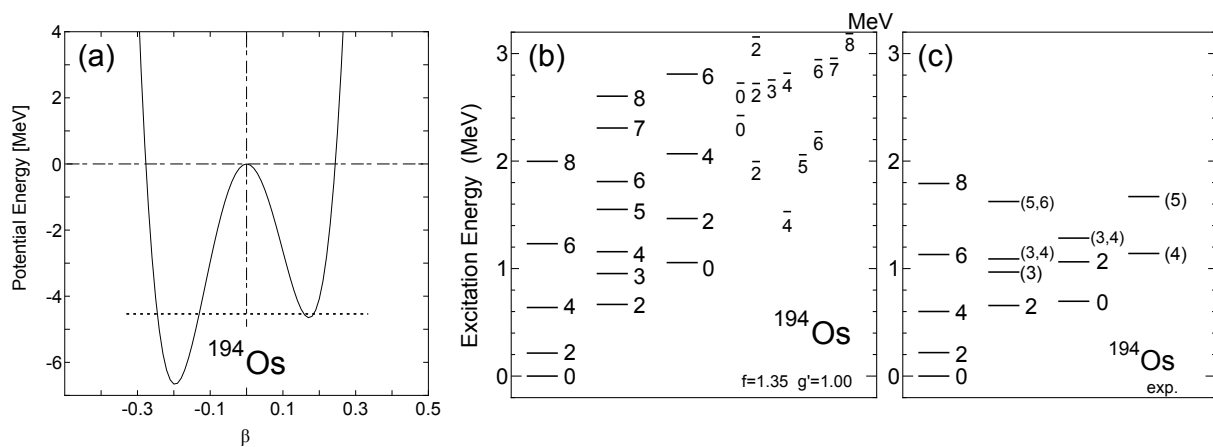


**Figure 5.** Same as Fig. 3 but for  $^{194}\text{Os}$ . Experimental data are taken from Ref.[28].

#### 4. Summary and conclusions

The low-lying quadrupole collective states of even-even osmium isotopes in the  $A \sim 190$  region are studied by means of the boson expansion theory with the self-consistent effective interactions. Potential surfaces are illustrated and theoretical energy levels are compared with experimental data. For  $^{192}\text{Os}$ , the structures of the BET wave functions are presented showing the degree of convergence of the present calculations, and the theoretical electro-magnetic properties are compared to available experiments resulting in reasonable agreements.

The theoretical potential of  $^{192}\text{Os}$  has two axial minima, one on the prolate side and the other on the oblate side with almost the same depth, which suggests strong  $\gamma$  instability. The evolution of the BET potential with changes in the number of neutrons suggests a prolate-oblate shape transition at around  $N = 116$  for osmium isotopes, which is compatible with the prediction of Refs. [1, 2].

#### References

- [1] P. Sarriguren, R. R.-Guzmán and L. M. Robledo, Phys. Rev. C **77**, 064322 (2008).
- [2] L. M. Robledo, R. R.-Guzmán and P. Sarriguren, J. Phys. G **36**, 1 (2009).
- [3] N. Al-Dahan *et al.*, Phys. Rev. C **85**, 034301 (2012).
- [4] T. Kishimoto and T. Tamura, Phys. Rev. C **27**, 341 (1983).
- [5] A. Klein and E. R. Marshalek, Rev. Mod. Phys. **63**, 375 (1991).
- [6] H. Sakamoto and T. Kishimoto, Nucl. Phys. **A501**, 205 (1989); **A501**, 242 (1989).
- [7] H. Sakamoto, J. Phys.: Conf. Series **1023**, 012003 (2018).
- [8] H. Sakamoto, Phys. Rev. C **93**, 034315 (2016).
- [9] H. Sakamoto, Acta Phys. Pol. B **48**, 573 (2017).
- [10] H. Sakamoto, Phys. Rev. C **52**, 177 (1995).
- [11] H. Sakamoto, Phys. Rev. C **64**, 024303 (2001).
- [12] S. G. Nilsson, C. F. Tsang, A. Sobiczewski, Z. Szymański, S. Wycech, C. Gustafson, I.-L. Lamm, P. Möller and B. Nilsson, Nucl. Phys. **A131**, 1 (1969).
- [13] B. R. Mottelson, *Nikko Summer School Lectures*, (NORDITA, Copenhagen, 1967) pub.288.
- [14] A. Bohr and B. R. Mottelson, *Nuclear Structure*, Vol. II (Benjamin, New York, 1975).
- [15] T. Kishimoto, J. M. Moss, D. H. Youngblood, J. D. Bronson, C. M. Rozsa, D. R. Brown and A. D. Bacher, Phys. Rev. Lett. **35**, 552 (1975).
- [16] T. Kishimoto, *Proc. Int. Conf. on Highly Excited States in Nuclear Reaction* (RCNP, Osaka 1980) p.145; p.377
- [17] T. Kishimoto, T. Tamura and T. Kammuri, Prog. Theor. Phys. Suppl. **74&75**, 170 (1983).
- [18] E. R. Marshalek, Phys. Rev. Lett. **51**, 1534 (1983); Phys. Rev. C **29**, 640 (1984); Phys. Lett. **244B**, 1 (1990).
- [19] H. Sakamoto and T. Kishimoto, Phys. Lett. **245B**, 321 (1990).
- [20] H. Sakamoto and T. Kishimoto, Nucl. Phys. **A486**, 1 (1988); **A528**, 73 (1991).
- [21] H. Feshbach, Ann. of Phys. **5**, 357 (1958); **19**, 287 (1962).
- [22] T. Kishimoto and T. Tamura, Nucl. Phys. **A270**, 317 (1976).
- [23] C. M. Baglin, Nuclear Data Sheets **113**, 1871 (2012).
- [24] M. V. Hoehn, E. B. Spera, H. D. Wohlfahrt, Y. Yamazaki, R. M. Steffen and R. K. Sheline, Phys. Rev. C **24**, 1667 (1981).
- [25] C. Y. Chen, J. X. Saladin and A. A. Hussein, Phys. Rev. C **28**, 1570 (1983).
- [26] C. S. Lim, R. H. Spear, W. J. Vermeer, M. P. Fewell and G. J. Gyapong, Nucl. Phys. **A485**, 399 (1988).
- [27] B. Singh, Nuclear Data Sheets **99**, 275 (2003).
- [28] T. Daniel *et al.*, Phys. Rev. C **95**, 024328 (2017).